Fabrication of a Lithium Sensor Based on LiYO$_2$ by Liquid Phase Processing

JIAN WU, LUIS YAMARTE & ANTHONY PETRIC

Department of Materials Science and Engineering, McMaster University, Hamilton, Ontario, Canada L8S 4L7

Abstract. A galvanic cell was constructed to measure the activity of lithium in liquid alloys. LiYO$_2$ solid electrolyte tubes were made by slip casting. Y$_2$O$_3$-12.5% MgO was selected as the lid composition due to its inertness to molten lithium and optimum strength. The tube and lid were joined by reaction bonding in which Li$_2$CO$_3$ acts as the bonding agent and also plays an important role as sintering additive. The tube-lid assembly was used in a galvanic cell to measure the emf of Li in Li-Sn and Li-Zn alloys at temperatures of 240–720°C. The emf results demonstrated the reproducible functioning of the sensor.

Introduction

The EMF technique is a well-known method for determining thermodynamic properties. For high temperature applications, solid electrolytes based on ceramic materials are required [1]. Although very precise measurements are possible by the EMF method, a suitable solid electrolyte must be found with sufficient ionic conductivity and stability to the electrode materials.

In determining the properties of Na, K and Rb containing alloys by the EMF technique, β-alumina was found to be an excellent solid electrolyte [2–4]. For Li alloys, however, Li β-alumina cannot be used as the electrolyte because it is not stable to metallic lithium. Most alternative ceramics that have been identified as potential solid electroytes [5] are also unstable to pure lithium (Li$_4$SiO$_4$, Li$_3$PO$_4$) or are hygroscopic (Li$_5$AlO$_4$, Li$_2$ZrO$_3$, Li$_8$ZrO$_6$). Of the materials discussed in [5], LiYO$_2$ appears to be the most practical and best in terms of phase stability.

Lithium yttrate is monoclinic with a slightly distorted NaCl structure that consists of mixed cation layers between layers of close-packed O^{-2} [6]. The cell parameters are $a = 6.12$, $b = 6.19$, $c = 6.21$ and $\beta = 118.8°$ [7]. Although Hoppe [8] initially reported that LiYO$_2$ had a tetragonal structure, later work by Waintal and Gondrand [9] and Stewner and Hoppe [10] showed that even low levels of impurity could stabilize the higher order structure. The structure of the pure crystal is monoclinic up to at least 1100°C, as are most compounds of the type LiREO$_2$ (RE signifies rare earth), and all belong to the same space group (P2$_1$/c). The conductivity of LiYO$_2$ was reported to be 3×10^{-3} S/cm at 400°C in the monoclinic form whereas the tetragonal form had a conductivity 1–2 orders of magnitude lower [11].

Successful experiments using the EMF technique require construction of a practical cell as has been described in the literature. For example, a slip casting procedure outlined by Rivier and Pelton [12] was widely used to fabricate β-alumina tubes. After sintering, the tubes were joined to α-alumina lids with a glass seal. The cells could then be assembled and used for emf measurements of alkali metal alloys.

However, when working with lithium alloys, α-alumina is not an acceptable lid material. A study of ceramics exposed to molten lithium revealed significant degradation of Al$_2$O$_3$ but good performance by MgO, Y$_2$O$_3$, AlN, BeO, UO$_2$ and ThO$_2$ [13]. In addition to chemical stability, matching thermal expansion is an important factor, and the selection of a lid material must take both factors into account.

Finally, for joining the tube and lid, an appropriate method is needed Silicate glass cannot be used because silica is not stable to lithium. In this study, we identified a MgO-Y_2O_3 composite as the optimum lid material and used reactive liquid phase sintering to join the lid and tube for use as an electrochemical cell. Practical usefulness of the cell was demonstrated by emf measurements of the Li-Sn and Li-Zn alloy systems.

Experimental Procedure

$LiYO_2$ was synthesized by solid state reaction of $LiNO_3$ (Caledon Laboratories Ltd.) or Li_2CO_3 (BDH Laboratory Supplies) and Y_2O_3 (Pacific Industrial Development Corp.). The chemicals were weighed, mixed in an alumina mortar, and pressed into pellets. The pellets were reacted in an alumina crucible and calcined by slowly heating to 725°C, holding for 4 h, then heating at 1200°C for 15 h.

The pellets were then crushed, mixed with 3 wt% (5 mol%) extra Li_2CO_3 and vibro-milled dry with alumina balls in a plastic bottle for 48 h. The particle size must be reduced to less than 5 μm to obtain a stable suspension and to minimize the porosity of the finished product. A suspension was prepared by mixing 72 g of the powder with 100 ml of absolute ethanol. The suspension was slip cast into alumina powder molds. The green tubes produced were 12 mm in diameter with a 1 mm wall thickness and a density 60% of theoretical.

Lids for the cells were pressed to yield final dimensions of approximately 19 mm diameter by 10 mm thick after sintering at 1670°C for 8 h. This resulted in an impervious fired body. The lids were then precisely machined with flat parallel ends, a 3 mm central bore, and a 45° countersink from one end. The hole was used for loading the cell and provided the electrical feed-through. The countersink was fitted with a Ta plug and mechanically sealed as described later.

Results and Discussion

Selection of the Lid Material

The objective of this study was to develop a sensor based on the $LiYO_2$ solid electrolyte to be used for measuring the chemical potential of lithium alloys. The cell must be impervious to gas leakage (hemetically sealed) but maintain sufficient ionic conductivity to allow

coulometric titration of lithium. The lid material must be an electrical insulator, non-reactive with lithium, and strong enough to support the load of mechanical clamping needed to close the cell. Furthermore, the thermal expansion coefficient must match that of $LiYO_2$. Of the ceramics compatible with lithium metal [14], MgO and Y_2O_3 are the most practical in terms of cost and ease of use. The thermal expansion coefficients of Y_2O_3 and MgO are reported as 9.3×10^{-6} K^{-1} and 13.5×10^{-6} K^{-1} respectively [15], compared to our measured value for $LiYO_2$ of 11.8×10^{-6} K^{-1}.

However, neither of the two simple oxides gave suitable results. Poor bonding was obtained between MgO lids and the $LiYO_2$ tubes, possibly due to the thermal expansion mismatch. Commercial Y_2O_3 powder is difficult to sinter. Our Y_2O_3 lids sintered at 1600°C were brittle and broke under pressure during tightening of the cell holder. The same problem occurred when we used $LiYO_2$ or $LiAlO_2$ as the lid material. We also tried Al_2O_3 and YAG which had high strength but reacted with molten lithium. Our solution was to test MgO as a sintering aid to Y_2O_3 in amounts of 5 to 15 wt%. Lids of various compositions were tested by clamping them in the cell holder as well as by exposure to molten lithium at 500°C for sixty days. None was attacked or infiltrated by lithium. It was observed that the strength of Y_2O_3 improved with MgO addition up to 12.5 wt% which was consequently selected as the optimum composition.

The Joining Process

Considerable effort was expended in developing a technique for joining the lid and tube. Initially, sealants such as $LiYO_2$, Li_2SiO_3, LiF and Li_2CO_3 were employed to join fully sintered lids and tubes. This approach met with persistent failure either because of incomplete sealing of the joint or because of an unexplained phenomenon of spontaneous cracking of the tube tip upon removing the cell from the furnace after joining. The crack formation could be delayed by storing the cell in a desiccator; thus, a reaction of free Li_2O with humidity was the most probable explanation. However, varying the composition from excess Li_2O to excess Y_2O_3 in the tube could not eliminate the problem.

We subsequently developed the following technique. Tubes were slip cast from powder containing $LiYO_2$ mixed with 3 wt% Li_2CO_3. The tubes were presintered at 1250°C for 0.5 h, buried in coarse $LiYO_2$
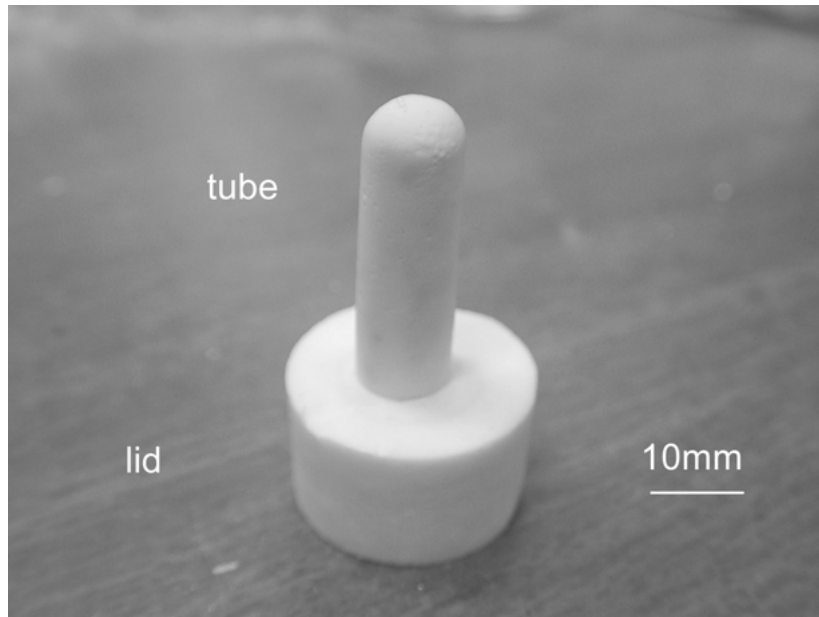
Fig. 1. LiYO$_2$ tube coupled to Y$_2$O$_3$-12.5% MgO lid.

powder to minimize lithium losses. The density after pre-sintering was measured by the Archimedes method in ethanol to be about 80% of theoretical, that is, about 3 g/cm^3 on average.

The tube was cut to a length of 3 cm. The tube was set on the lid as shown in Fig. 1 and loaded into a SiC furnace, preheated to 1300°C. The lid/tube couple could be viewed during the bonding process through a view port in the door. When the gap between the tube and lid, observed as a dark line, closed completely, the furnace was shut off (allowing sintering to continue). The furnace temperature was approximately 1325°C when joining occurred. Near 1325°C, shrinkage easily visible to the eye started at the bottom of the tube and propagated as a wave to the top in a span of 30–60 s (Fig. 2). The tube was removed from the furnace at this point and allowed to air cool. If the heating was
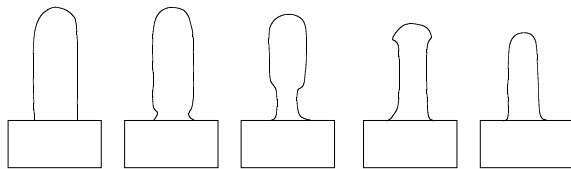

Fig. 2. Sintering of the tube propagated from the bottom to the top in approximately 1 min.

continued, the tube quickly softened and collapsed under its own weight, although the joint remained intact (Fig. 3).

This procedure effectively densified the tube and joined it to the lid. Figure 4 shows the sintered microstructure of the tube with approximately 98% density. The joint between the tube and the lid is shown in Fig. 5. The inset shows a fine-grained LiYO$_2$ phase has formed between the larger Y$_2$O$_3$ grains in the lid. The joint was normally found to be impervious by helium leak testing to a level of 10^{-4} mbar.

Mechanism of the Joining and Sintering Process

A hypothesis for the joining and sintering mechanism is proposed, based on DTA/TGA measurements and by comparison with data from the Li$_2$O-Al$_2$O$_3$-CO$_2$ phase diagram. Although phase equilibria in the Y$_2$O$_3$-rich portion of the system have been reported [16], no data are available for the Li$_2$O-LiYO$_2$ part of the diagram. Note that LiYO$_2$ is the only intermediate compound formed between Li$_2$O and Y$_2$O$_3$.

DTA of pre-sintered tubes showed three peaks during heating from room temperature to 1500°C. In order to obtain clarification of the peaks, a control DTA experiment was performed, using a 1:1:0.2 mixture of LiYO$_2$, Y$_2$O$_3$ and Li$_2$CO$_3$.
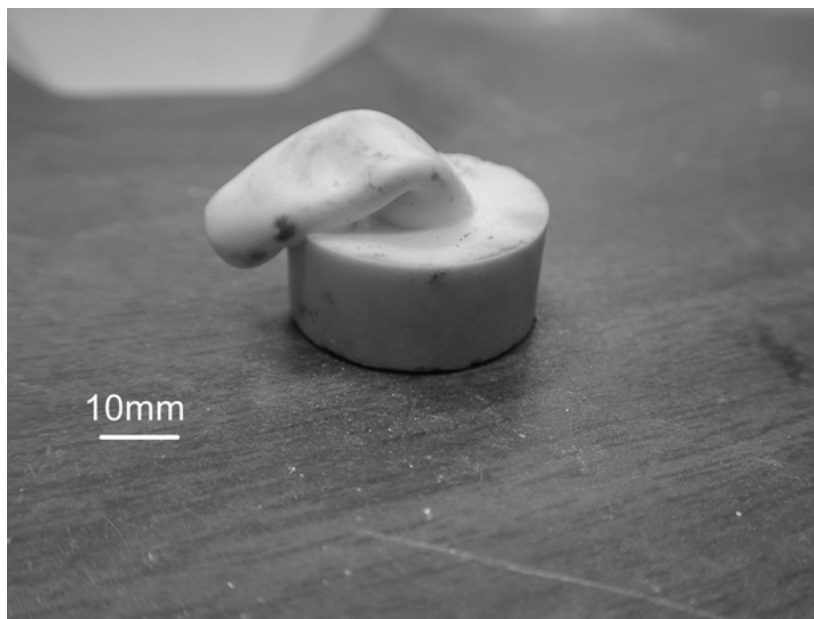
Fig. 3. Over-heating above 1325°C resulted in collapse of the tube but the joint remind intact.
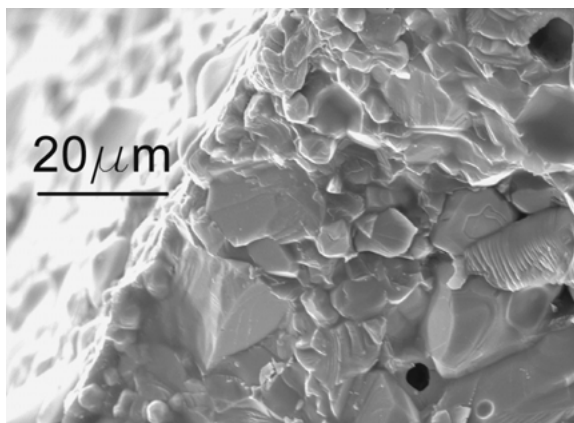

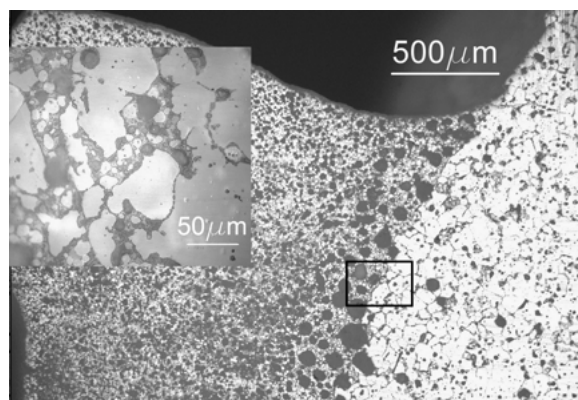*Fig. 4.* Microstructure of a fractured section of LiYO$_2$ tube revealing high sintered density.

Fig. 5. Polished section showing joint formed between LiYO$_2$ tube (left) and Y$_2$O$_3$-12.5% MgO lid (right). Note high residual porosity in the tube near the joint. Inset shows large Y$_2$O$_3$ grains infiltrated by fine LiYO$_2$ formed by liquid phase reaction at the interface.

The control sample was thermally cycled twice from room temperature to 1500°C. The DTA curve showed three endothermic peaks during the first heating (Fig. 6), but no peaks appeared in the second run. The first peak corresponded to the melting of Li$_2$CO$_3$ at 723°C. The second event in the analysis began at 750°C and lasted until 950°C. It was accompanied by a large decrease in sample weight, as seen by TGA. This can be explained by the calcination of lithium carbonate (accompanied by loss of CO$_2$), followed by reaction of the liberated Li$_2$O with free Y$_2$O$_3$ to form LiYO$_2$. DTA shows that the latter exothermic reaction began near 920°C. A third peak at 1180°C cannot be explained, but did not occur when an Ar atmosphere was used. The lack of peaks in the second run is attributed to the disappearance of Li$_2$CO$_3$ during the first DTA cycle.
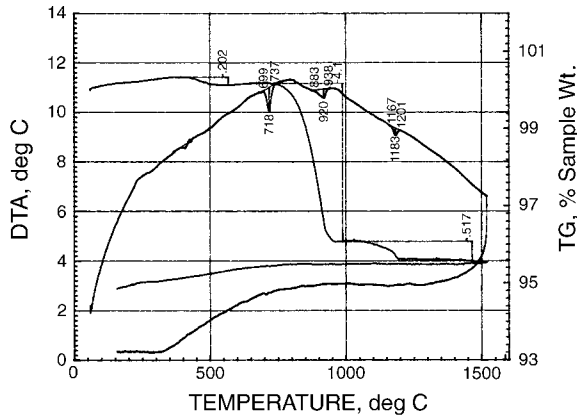
Fig. 6. DTA and TGA analysis of a 1:1:0.2 mixture of $LiYO_2$, Y_2O_3 and Li_2CO_3.

This information can be used to explain how the sintering/bonding process occurs. The lid material has a large Y_2O_3 content. The tube is nominally $LiYO_2$ with 3 wt% Li_2CO_3 although we have observed that some of the $LiYO_2$ is converted to Li_2CO_3 or LiOH during

preparation of the slip and pre-sintering. The calcination temperature of Li_2CO_3 is very sensitive to the CO_2 pressure. Thus, at the usual pressure of $10^{-3.4}$ atm CO_2 in the atmosphere, decomposition begins shortly above the melting point (Fig. 7). On the other hand, at a pressure of 0.5 atm, Li_2CO_3 remains a stable liquid above the usual ceramic processing temperatures used in this study. The slow heating of a DTA experiment represents the former condition; rapid firing as in the case of our sintering cycle parallels the latter, i.e., a CO_2-rich atmosphere envelopes the sample during heating.

To test this theory, we repeated the DTA/TGA run with a mixture of Li_2CO_3 + $LiYO_2$ in a pure CO_2 atmosphere (Fig. 8). No weight loss occurred until 1100°C and the only significant reaction to this point was the melting of Li_2CO_3. The exothermic peak above 1300°C is due to reaction with the alumina crucible and did not occur with a Pt crucible. Another important factor is that it took 20 min to heat the sample from 1100 to 1300°C during the DTA run (10°/min), but only 2–3 min in the sealing procedure. This results in a considerable difference of CO_2 loss between the
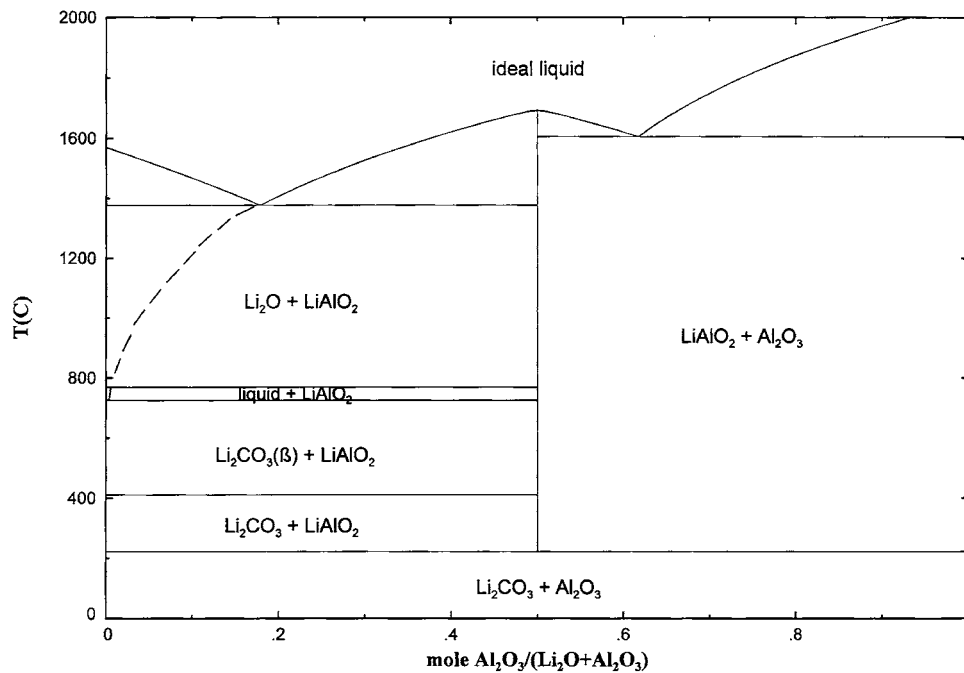

Fig. 7. Li_2O-Al_2O_3-CO_2 phase diagram at 400 ppm CO_2. Dashed line shows liquidus when Li_2CO_3 is stable over the temperature range of the diagram at a CO_2 pressure of 0.5 atm (ref. [17]).

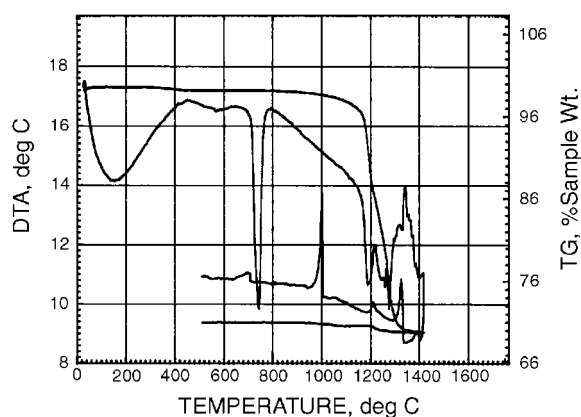*Fig. 8.* DTA and TGA analysis of a 1:1 mixture of LiYO$_2$, and Li$_2$CO$_3$ in CO$_2$ atmosphere.

two cases, especially since the tube is compact and the DTA sample is loose powder.

During the rapid firing process, the Li$_2$CO$_3$ forms a liquid phase which undergoes calcination slowly relative to the heating rate as the temperature approaches 1300°C. We can model the Li$_2$O-Y$_2$O$_3$-CO$_2$ system by the very similar Li$_2$O-Al$_2$O$_3$-CO$_2$ system for which we have solid phase data [17] and we can model the liquid phase by an ideal solution (Fig. 7). The model diagram shows that a eutectic forms at 725°C between Li$_2$CO$_3$ and LiYO$_2$. As the CO$_2$ pressure increases, the Li$_2$CO$_3$ is stabilized to higher temperatures, until at 0.5 atm CO$_2$, the liquidus forms a continuous curve from the low eutectic up to the high temperature liquid (as shown by the dashed line). If Li$_2$CO$_3$ does not decompose to Li$_2$O, as we expect, the volume fraction of liquid increases with temperature. When sufficient liquid phase fraction is present, the melt at the base of the tube reacts with the Y$_2$O$_3$ lid to form a solid LiYO$_2$ joint. This coincides with a rapid densification process that propagates upward to the top of the tube. We anticipate that this sintering stage involves a reaction of the melt with excess Y$_2$O$_3$ in the tube, which has been observed by SEM as a plate-like surface coating (Fig. 9).

The result after cooling is a near theoretical density tube and a fully integrated solid joint. The high density of the tube is due to the presence of liquid Li$_2$CO$_3$ that we believe is not fully calcined during rapid firing and is retained as a solid grain boundary phase after cooling. Another interesting phenomenon that can be observed is a string of pores near the edge of the lid in contact with the tube (Fig. 5). Our explanation for this
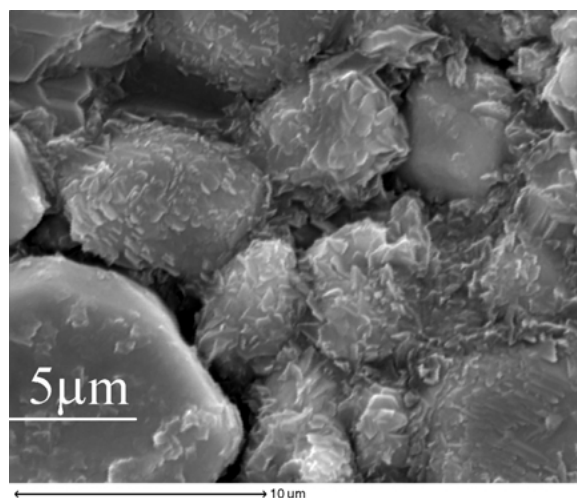

Fig. 9. SEM image of pre-sintering microstructure of LiYO$_2$ tube showing irregular surface deposit of Y$_2$O$_3$.

porosity is that near the joint, liquid was drawn from tube to react with the lid, leaving behind a volume of space which could not be eliminated in the short sintering time. Furthermore, the formation of solid LiYO$_2$ during the reaction pins the tube to the lid and prevents shrinkage of the tube diameter at the base.

Stability of LiYO$_2$

The sintering of LiYO$_2$ tubes as described above resulted in a product with very good stability. It maintained structural integrity in air for more than 2 years, as well as in contact with molten Li for several months. However, this does not imply phase purity of the LiYO$_2$ tube.

The thermodynamic properties of LiYO$_2$ are not available. XRD analysis showed the pure LiYO$_2$ pattern only for the fresh powder formed by reaction of Li$_2$CO$_3$ and Y$_2$O$_3$. After any further treatments, e.g., reheating the powder in air or recovering powder from dried ethanol slip or from pre-sintered tubes, XRD analysis revealed the presence of Y$_2$O$_3$, formed by decomposition of LiYO$_2$ (Fig. 10). No Li$_2$O, Li$_2$CO$_3$ or LiOH could be detected by XRD.

However, DTA gave evidence for the existence of LiOH and Li$_2$CO$_3$ by way of endothermic peaks near 400 and 710°C, corresponding to the melting points of these compounds. Hence, we may conclude that LiYO$_2$ is not stable in air. Others have observed that LiYO$_2$ decomposed in air below 300°C [18]. The
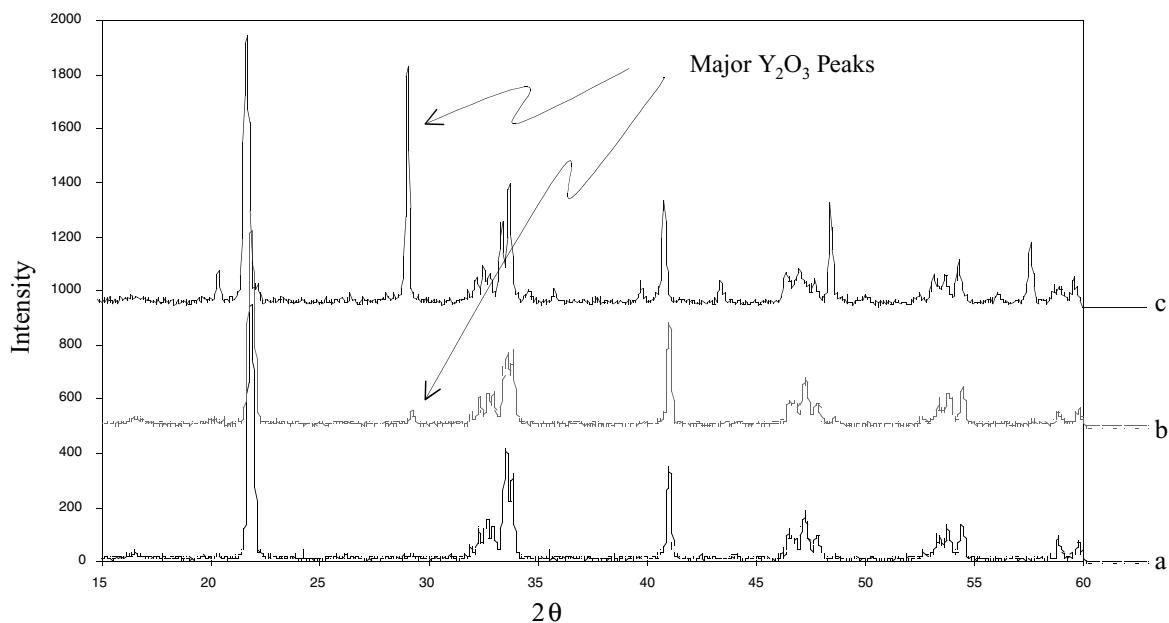
Fig. 10. XRD spectrum of LiYO$_2$: (a) freshly synthesized powder, (b) powder recovered from slip before casting, and (c) after pre-sintering.

thermodynamic data also show that LiAlO$_2$ is unstable at low temperatures [17], reacting with CO$_2$ in air to form Li$_2$CO$_3$.

The presence of Li$_2$CO$_3$ is not detrimental for our application. Li$_2$CO$_3$ is known to have good electrolytic properties [19]. Furthermore, it is instrumental in sintering and sealing our electrochemical cell. TGA of a tube after the sealing procedure revealed an endothermic peak at the melting of Li$_2$CO$_3$, indicating its presence was maintained.

LiYO$_2$ tubes with no Li$_2$CO$_3$ additive could not be used to make a cell. No significant strength was observed in the joint, although some reaction was evident. Densification occurred only when the tube was heated above 1500°C, and showed only incomplete solid phase sintering behavior. The tube spontaneously cracked within minutes of being exposed to air after cooling (Fig. 11), as described earlier.

The optimum amount of Li$_2$CO$_3$ added to the LiYO$_2$ powder before slip casting was found to be 3 wt%. A larger amount of Li$_2$CO$_3$ resulted in cracking of the cell upon cooling, and less Li$_2$CO$_3$ did not yield a good seal.

The furnace temperature and heating time were critical. Over-heating resulted in collapse of the tube (Fig. 3). Also, if the heating rate was too slow, we could not obtain a good seal since the Li$_2$CO$_3$ de-

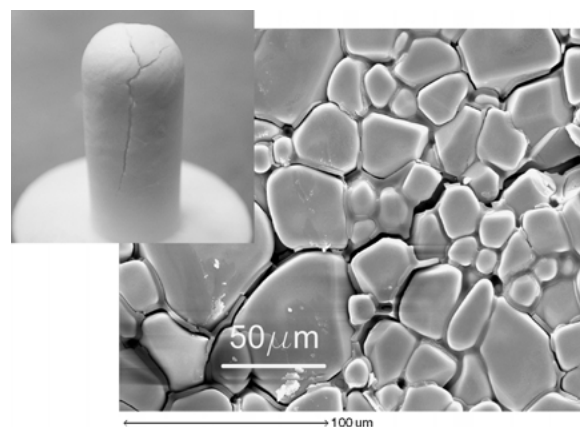*Fig. 11.* Tube sintered from LiYO$_2$ powder with no additives spontaneously cracked when cooled and exposed to air.

composed before bonding. A second heating of the tube above 1300°C generally caused blistering and cracking (Fig. 12), probably due to decomposition of Li$_2$CO$_3$.

Galvanic Cell Testing

EMF measurements were taken between working and reference half-cells that were electrically connected by
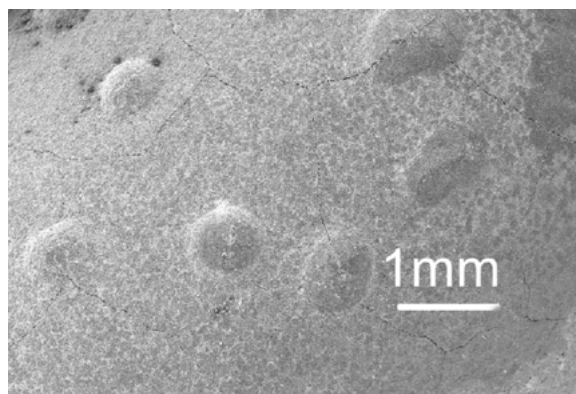
Fig. 12. Bloating and cracking of tube surface after reheating to 1300°C, caused by the decomposition of Li_2CO_3.

means of a molten metal bath. The half-cells were constructed by adding electrode materials to the tube-lid assembly via the bore. The cell was closed with a Ta cone tapered to fit the countersink in the lid. A Ta wire lead completed the circuit. The Ta cone was clamped to the lid by a cell holder (Fig. 13) machined from a Zr-2.5% Nb alloy supplied by Atomic Energy of Canada Ltd.

The following electrochemical cells were assembled and tested:

(−) Ta, Li | $LiYO_2$ | Sn-Li, Ta (+)
(−) Ta, Li-Sn | $LiYO_2$ | Li-Zn, Ta (+)

The half-cells were immersed in a molten Sn-1%Li bath which served as a sink and source of Li during coulometric titration. All experiments were done in a high purity Ar atmosphere glove box.

The reference electrodes used to study the Li-Zn system were Sn-0.635 at% Li and 1.62 at% Li alloys. Tin was chosen as the base metal for the reference electrode because of its low melting point and low vapor pressure. Use of a dilute lithium composition also ensured a low Li vapor pressure, reducing the chances of side-reactions or leakage. The reference electrodes were calibrated against pure Li versus temperature between 340 and 680°C. The emf for each of the compositions is given as follows:

$$0.635 \text{ at\% Li: E (mV)} = 645.9 + 0.51985$$
$$1.62 \text{ at\% Li: E (mV)} = 784.1 - 0.212\,T$$
$$+ 0.0007T^2\ (T°C)$$

The calibration curves shown in Fig. 14 for the 2 reference cells represent points from several temperature cycles and show good reproducibility. Our results are consistent with literature data at higher lithium concentration [20–22].

Next, the emf of the Li-Zn alloy was measured as a function of composition at 600°C. The composition of the Li-Zn electrode was varied by coulometric titration. A titration current of 0.1 mA could be passed at 600°C

Conducting wire (Ta)

Tight screw (Ta)

Insulator tube (Al_2O_3)

Holder(Zr-2.5%Nb)

Insultor lid (Y_2O_3)

Insulator gasket (Al_2O_3 or Y_2O_3)

Cell tube ($LiYO_2$)
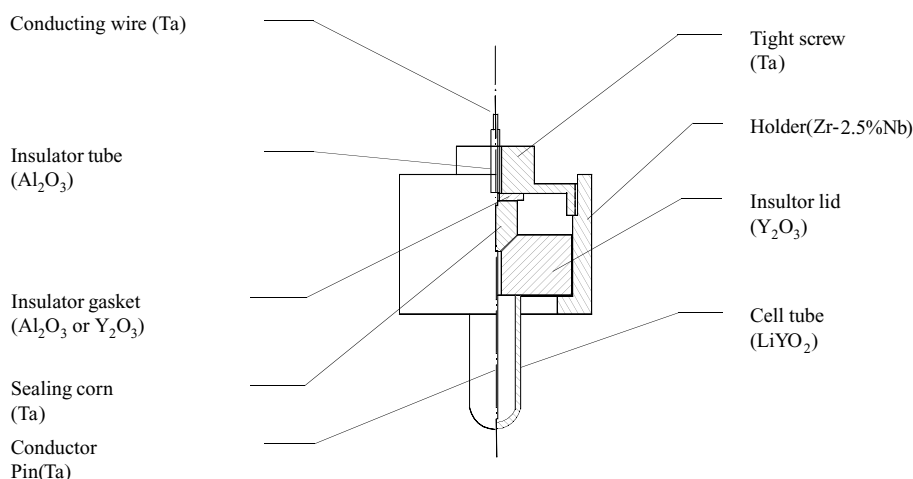
Sealing corn (Ta)

Conductor Pin(Ta)

Fig. 13. Final cell assembly with a Ta cone tapered to fit the countersink in the lid. A Ta lead completed the circuit. The Ta cone was clamped to the lid by a cell holder to provide a hermetic seal.
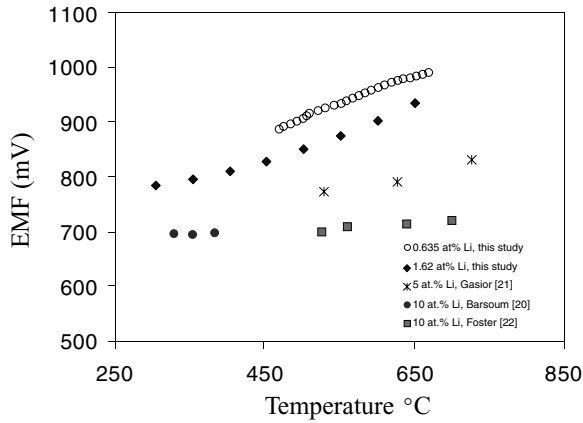
Fig. 14. EMF of tin-lithium alloys versus pure Li.

with an applied overpotential of 300 mV. Activities, activity coefficients and Gibbs energy of mixing are reported in Table 1. The EMF and activity coefficient of Li in Li-Zn alloys are plotted in Fig. 15 and show good agreement with a previous emf study of the Li-Zn system using a LiCl-LiF molten salt electrolyte [23].

Work involving measurement of the thermodynamic properties of the Al-Li system is in progress. To

Table 1. Thermodynamic properties of Li-Zn alloys at 600°C.

| X_{Li}	EMF (mV)	$Ln\gamma_{Li}$	a_{Li}	$Ln\gamma_{zn}$	a_{zn}	ΔG_{mix} (J/mol)
0.0011	892	−5.04	0.00001	0.00000	0.99890	−100
0.0015	855	−4.87	0.00001	0.00000	0.99850	−130
0.002	829	−4.81	0.00002	0.00000	0.99800	−170
0.004	752	−4.48	0.00005	0.00000	0.99600	−330
0.006	716	−4.41	0.00007	−0.00130	0.99271	−470
0.01	669	−4.29	0.00014	−0.00250	0.98753	−740
0.02	599	−4.05	0.00035	−0.00650	0.97365	−1350
0.025	575	−3.96	0.00048	−0.00870	0.96655	−1630
0.05	498	−3.63	0.00133	−0.02070	0.93054	−2900
0.075	439	−3.25	0.00291	−0.04490	0.88439	−4000
0.093	399	−2.93	0.00497	−0.07330	0.84290	−4710
0.1	391	−2.9	0.00550	−0.07660	0.83363	−4960
0.125	351	−2.59	0.00938	−0.11600	0.77917	−5820
0.155	314	−2.31	0.01539	−0.16130	0.71913	−6720
0.2	258	−1.82	0.03241	−0.26740	0.61229	−7830
0.25	214	−1.46	0.05806	−0.37250	0.51676	−8770
0.26	206	−1.39	0.06476	−0.39620	0.49793	−8910
0.28	188	−1.23	0.08184	−0.45510	0.45676	−9180
0.3	173	−1.1	0.09986	−0.50830	0.42106	−9410
0.32	158	−0.97	0.12131	−0.56670	0.38583	−9600
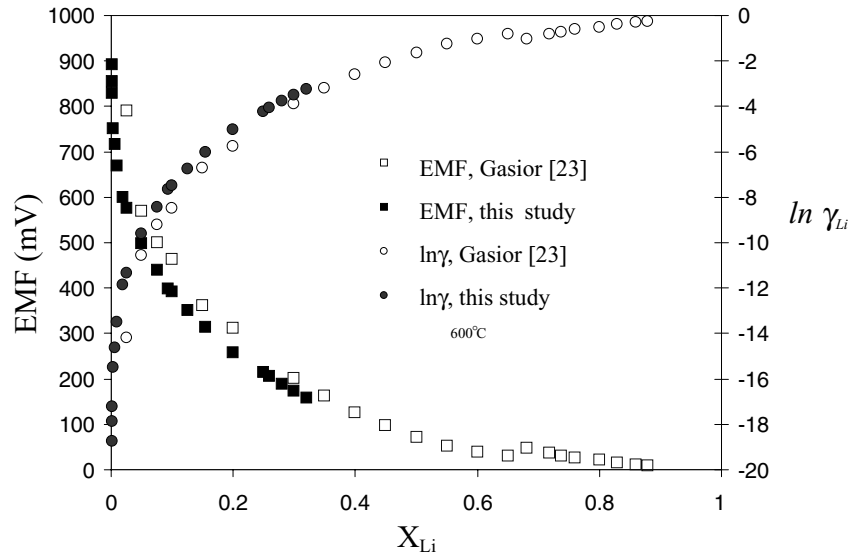
Fig. 15. Plot of EMF and lnγ_{Li} vs. X_{Li} for Li-Zn alloy at 600°C.

date, the cells have performed well with no noticeable reaction between the electrolyte and molten aluminum electrode.

Conclusions

A Li sensor was fabricated by reactive sintering and joining of a $LiYO_2$ tube with a Y_2O_3-12.5% MgO lid. Joining occurred by reaction of a liquid phase with Y_2O_3 to from solid $LiYO_2$. The joining process was followed by a rapid sintering of the tube, aided by the presence of liquid Li_2CO_3 and reaction with excess Y_2O_3 in the tube. The method depends on a rapid firing process to avoid decomposition of the carbonate and subsequent loss of the liquid phase. It may be possible to replace the rapid firing process by use of a controlled CO_2 atmosphere in order to maintain the Li_2CO_3 phase to high temperatures. Overheating of the sample results in excessive liquid phase formation and collapse of the tube.

The measured emf between the reference lithium alloy and lithium in zinc solution showed stable output between 240 and 720°C. Y_2O_3-MgO lids showed excellent chemical resistance to molten lithium as well as good mechanical properties.

Acknowledgments

References

1. J.N. Pratt, *Metall. Trans*. A, **21A**, 1223 (1990).
2. A. Petric, A.D. Pelton, and M.L. Saboungi, *Ber. Bunsenges, Phys. Chem.*, **93**, 18 (1989).
3. M.L. Saboungi, S.R. Leonard, and J. Ellefson, *J. Chem. Phys.*, **85**, 6072 (1986).
4. A. Petric, A.D. Pelton, and M.L. Saboungi, *J. Electrochem. Soc.*, **135**, 2754 (1988).
5. E.E. Hellstrom and W. Van Gool, *Solid State Ionics*, **2**, 59 (1981).
6. X. Zhang, D. Jefferson, and R. Lambert, *J. Catal.*, **141**, 583 (1993).
7. J. Lynch, C. Ruderer, and W. Duckworth, *Engineering Properties of Selected Ceramics Materials* (The American Ceramic Society, Battelle Memorial Institute, Columbus, Ohio, 1966).
8. R. Hoppe, *Angew. Chem.*, **71**, 457 (1959).
9. A. Waintal and M. Gondrand, *Mater. Res. Bull.*, **2**, 889 (1967).
10. V. Stewner and R. Hoppe, *Z. Anorg. Allg. Chem.*, **380**, 250 (1971).
11. Y. Zou and A. Petric, *Mat. Res. Bull.*, **28**, 1149 (1993).
12. M. Rivier and A.D. Pelton, *Am. Ceram. Soc. Bull.*, **57**, 183 (1978).
13. R.J. Lauf and J.H. DeVan, *J. Electrochem. Soc.*, **139**, 8 (1992).
14. G. Eichinger, *Solid State Ionics*, **2**, 289 (1981).
15. G.V. Samsonov, *The Oxide Handbook*, Second Edition (IFI Plenum Data Company, New York, 1982).
16. I.A. Bondar and L.N. Koroleva, *Russ. J. Inorg. Chem.*, **23**, 900 (1978); *Zh. Neorg. Khim.*, **23**, 1636 (1978).
17. C.W. Bale, A.D. Pelton, and W.T. Thompson, *FACTSage 5.0* (Ecole Polytechnique de Montreal/Royal Military College, Canada, 2001, http://www.crct.polymtl.ca).
18. I.A. Rozdin, H.T. Saripov, S.S. Plotkin, N.V. Brotnikov, T.B. Polueva, and K.I. Petrov, *Izv. Akad. Nauk SSSR Neorg. Mater.*, **12**, 863 (1976).
19. J. Mizusaki and H. Tagawa, *Solid State Ionics*, **53–56**, 791 (1992).
20. M.W. Barsoum and H.L. Tuller, *Metall. Trans. A*, **19A**, 637 (1988).
21. W. Gasior, Z. Moser, and W. Zakulski, *J. Non-Cryst. Solids*, **205**, 379 (1996).
22. M.S. Foster, C.E. Crouthamel, and S.E. Wood, *J. Phys. Chem.*, **70**, 3042 (1966).
23. W. Gasior and Z. Moser, *J. Chem Phys*, **90**, 387 (1993).